ISTITUTO NAZIONALE DI GEOFISICA E VULCANOLOGIA

Velocity profile report at the seismic station IV.MILN–Milano (MI)

Report sul profilo di velocità sismica per il sito della stazione sismica IV.MILN – Milano (MI)

Working Group: **Claudia MASCANDOLA** **Sara LOVATI** **Marco MASSA**	Date: Dicembre 2019
Subject: **Final report illustrating measurements, analysis and results for Vs profile at station IV.MILN**	

INDEX

1. INTRODUCTION

In this report, we present the geophysical measurements and the results obtained in the framework of the 2019-2021 agreement between INGV and DPC, Allegato B2, WP1 - TASK 2: "Caratterizzazione siti accelerometrici" (Coord.: G. Cultrera, F. Pacor). In this report, the results for station IV.MILN, belonging to the Italian National Seismic Network (RSN-INGV), are presented. The recording station is located in the metropolitan city of Milan, in the Po Plain area (Northern Italy).

Geophysical measurements consist in two ambient vibration array in 2D configuration that provide results in terms of resonance frequency of the soil deposits and in terms of dispersion curves of surface waves. These curves are inverted to obtain a shear-wave velocity (Vs) profile that is suitable for assigning the soil class according to the current Italian seismic code (NTC 2018) and the current Eurocode (EC8).

2. GEOPHYSICAL INVESTIGATIONS

Figure 1a shows the location of the IV.MILN seismic station (yellow triangle) and the location of the two microtremor arrays performed (yellow and red points). Figure 1b is a zoom on the array measurements. The smaller array (Array 1) has a radius of 12.5 m and it is reported with red points, whereas the bigger array (Array 2) has a radius of 50 m and it is reported with yellow points. The seismic sensors were positioned in a circular geometry in order to have a homogeneous azimuthal coverage that allows a better performance of the array techniques. The geographic coordinates of the array stations are reported in Table 1 for Array 1 and in Table 2 for Array2. The IV.MILN seismic station is 356 m far away from the center of the smaller array (Array 1 – MI06) and 270 m far away from the center of the bigger array (Array 2 – MI12).


IV.MILN
Via A. Corti
Via A. Vallisneri
Via A. Grossich
Via C. Beretta
Largo Volontari del Sangue
Via Ponzio
Via Carlo Pascal
Via Camillo Golgi
Via C. Clericetti
Via Bernardo Ugo Secondo
Via G. Celoria
Via C. Golgi
© 2018 Google
Google Earth

a)

b)

Figure 1: a) location of the IV.MILN seismic station (yellow triangle) and of the 2D array performed at the site. b) Zoom on the array measurements. The red points indicate the stations of the smaller array, with a radius of 12.5 m. The yellow points indicate the stations of the bigger array, with a radius of 50 m.

Station	Lat. [°]	Lon. [°]	El. [m]
MI01	45.47719	9.23390	118
MI02	45.47739	9.23397	118
MI03	45.47737	9.23374	118
MI04	45.47729	9.23372	118
MI05	45.47740	9.23385	118
MI06	45.47730	9.23387	118
MI07	45.47724	9.23400	118
MI08	45.47722	9.23376	118
MI09	45.47731	9.23403	118

Table 1: geographic coordinates of the Array 1 stations (WGS84).

Station	Lat. [°]	Lon. [°]	El. [m]
MI10	45.47781	9.23311	111
MI11	45.47751	9.23296	106
MI12	45.47782	9.23247	113
MI13	45.47816	9.23294	103
MI14	45.47828	9.23244	113
MI15	45.47816	9.23204	110
MI16	45.47782	9.23183	112
MI17	45.47749	9.23203	109
MI18	45.47737	9.23249	112

Table 2: geographic coordinates of the Array 2 stations (WGS84).

All stations of the array are equipped with Reftek-130 digitizer and Lennartz 3D-5s velocimetric sensors. The measurements were recorded in July and lasted more than two hours. A view of the fieldwork is shown in Figure 2a and 2b for Array1 and Array2 respectively.

a)

b)

Figure 2: fieldwork at the IV.MILN seismic station for Array1 (a) and Array2 (b).

2.1 ARRAY 1

The geometry of the Array 1 controls the response in terms of theoretical transfer function as described in Figure 3. On the left, the array transfer function is shown. On the right, the limits for the aliasing conditions are reported both in slowness and in velocity domains.

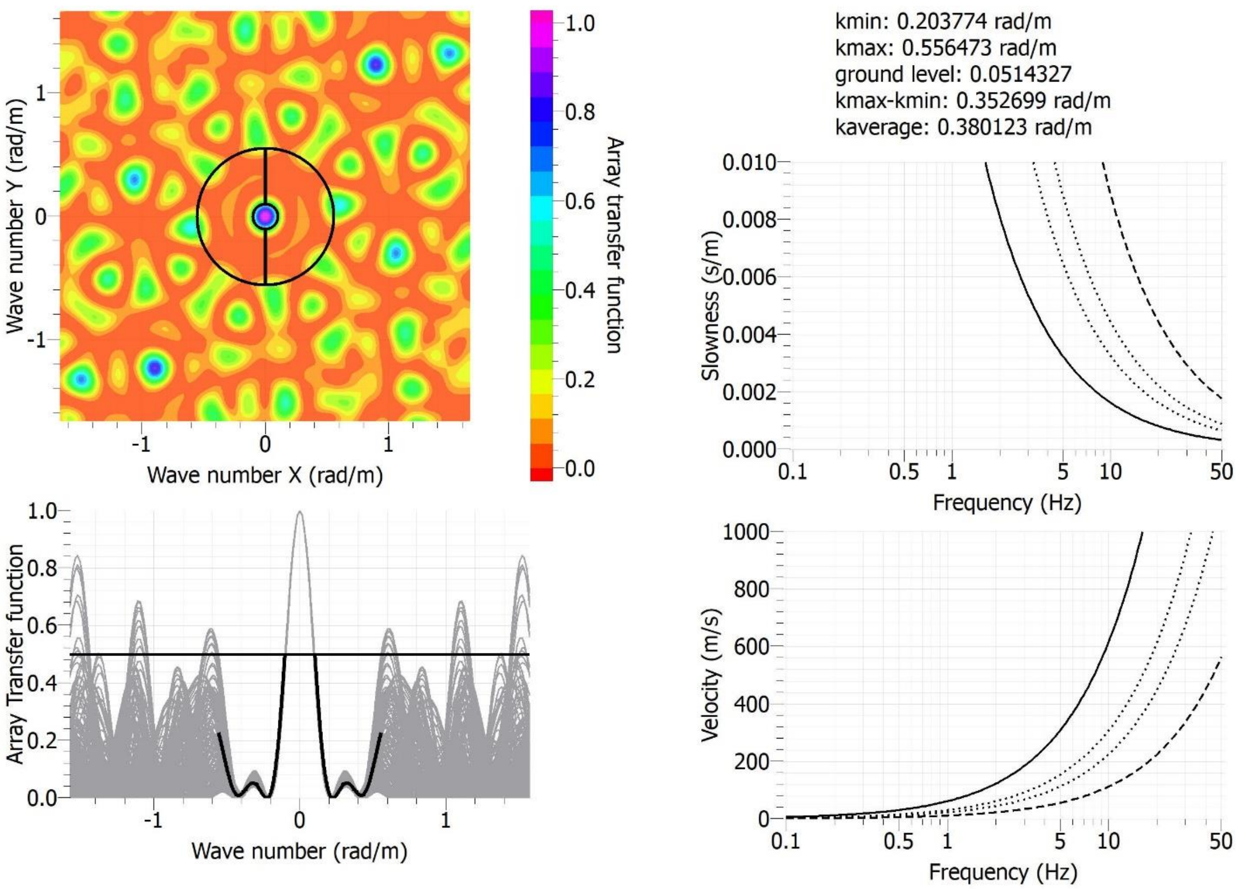

Figure 3: on the left, the theoretical array transfer function is reported for Array1. On the right, the aliasing conditions are reported in the slowness and velocity domains.

The H/V curves of the 9 stations are superimposed on each other in Figure 4, where the average H/V is reported in a solid black line and the corresponding standard deviation in dashed black lines. There is a general agreement of the H/V shapes showing a good overlapping in the frequency range 0.1-15 Hz. The H/V peak at 0.18 Hz (σ = 0.03 Hz) can be observed on all the H/V curves and it is probably due to a deep impedance contrast. However, Figure 4 shows a further amplification in the frequency range 0.4-0.6 Hz that can approach or exceed an amplitude of 2, one of the conditions for a clear H/V peak (SESAME Guidelines, 2004). The directional H/Vs from the 9 stations of Array 1 (Figure 5) do not show any polarization effect.

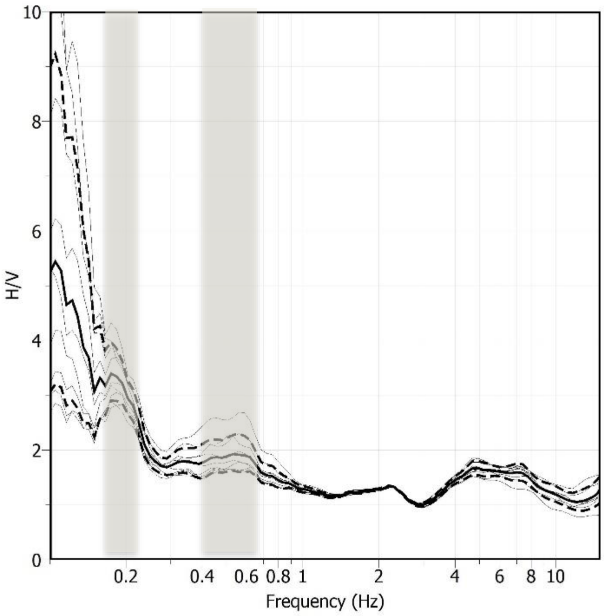

Figure 4: H/V curves of the 9 stations of Array 1. The average is reported with a solid black line, whereas the corresponding standard deviation is reported with dashed black lines.

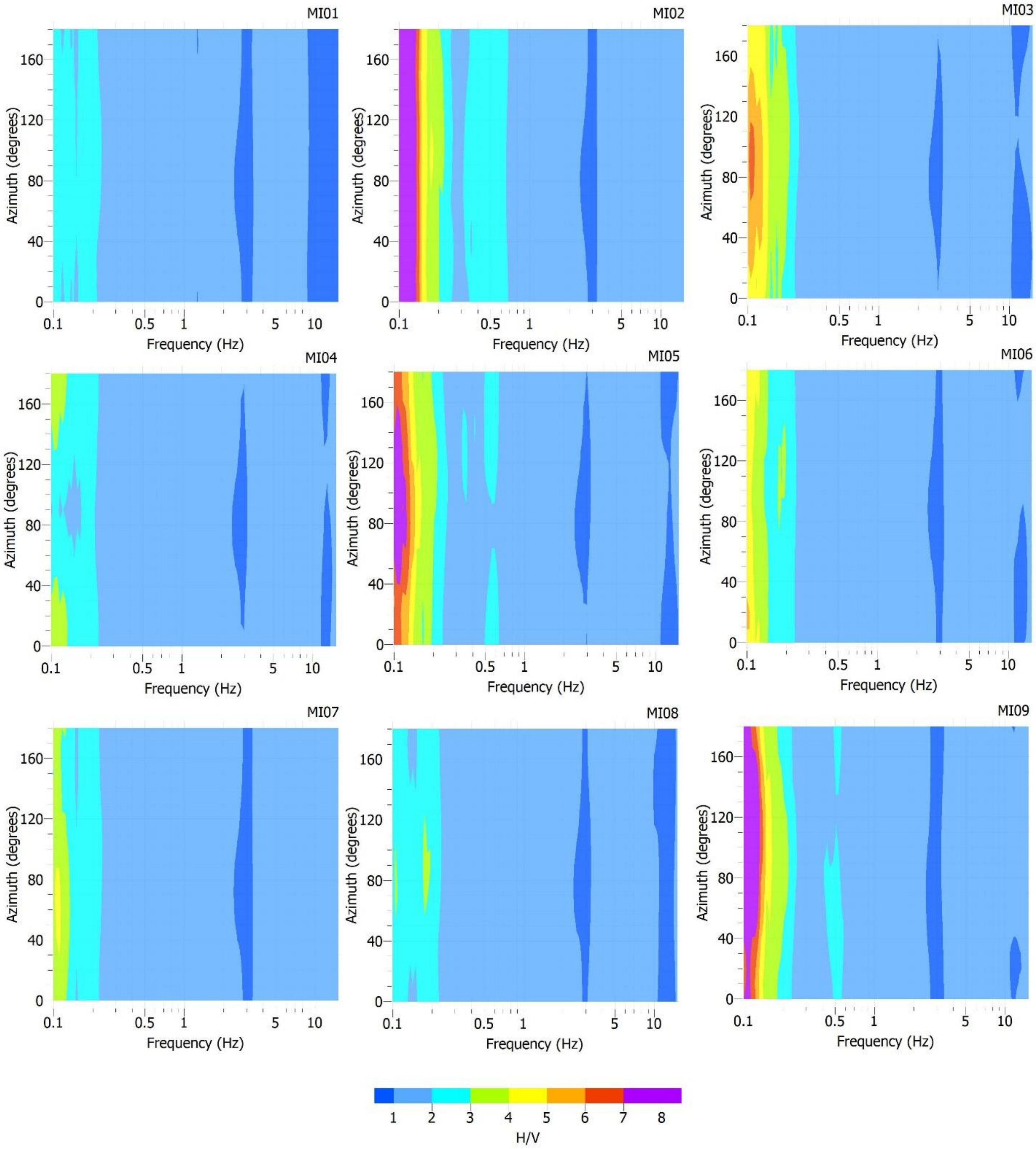

Figure 5: directional H/V for the 9 stations of Array 1.

Data from the 2D array have been analyzed with the GEOPSY code (http://www.geopsy.org) in terms of high-resolution FK analysis on all the three components (NS, EW, Z). The dispersion curves obtained from the Array 1 are shown in Figure 6a for the vertical components, 6b for the radial components and 6c for the transverse components. The vertical and radial components allow picking the Rayleigh wave dispersion curves, whereas the transverse components allow picking the Love wave dispersion curves. The aliasing conditions (black lines) constrain the validity range of the picked dispersion curves in the frequency range 8-20 Hz.

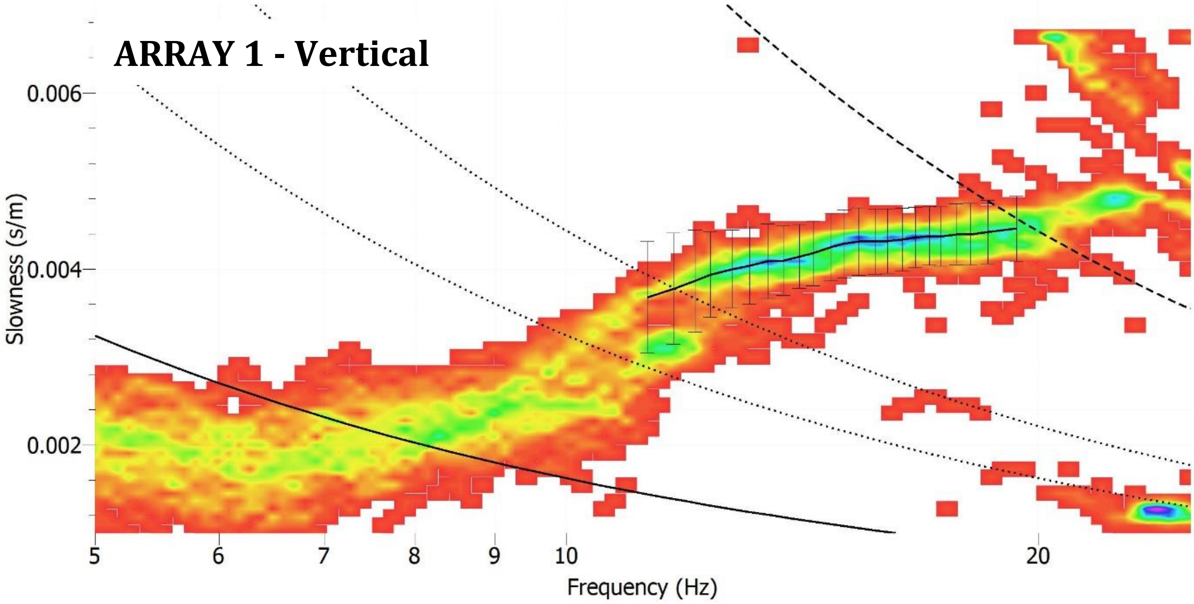

a)

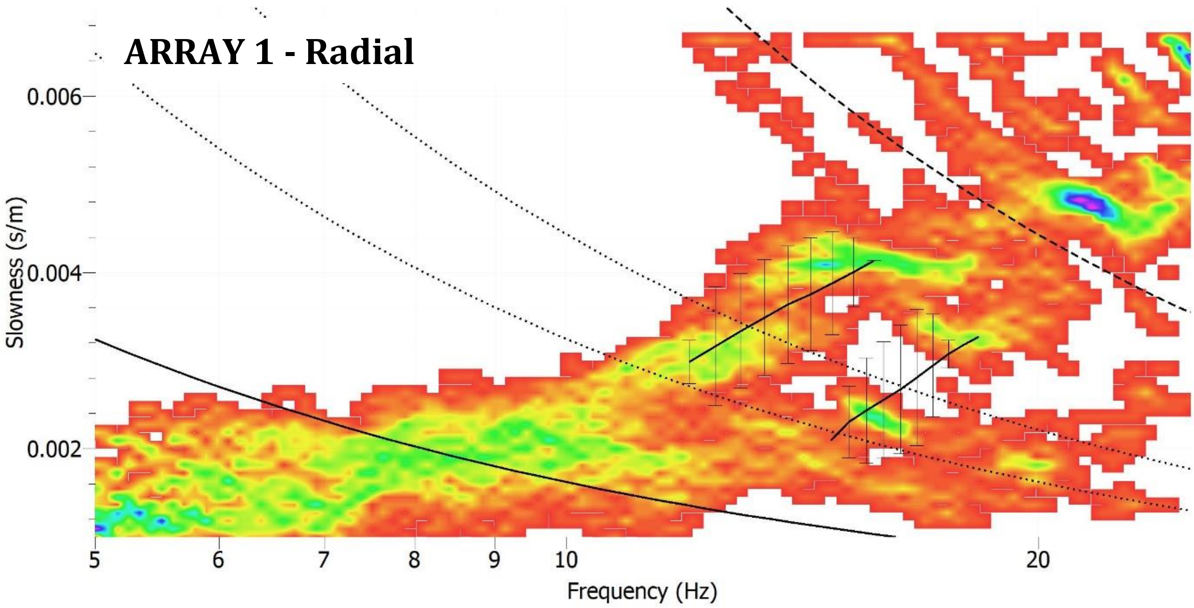

b)

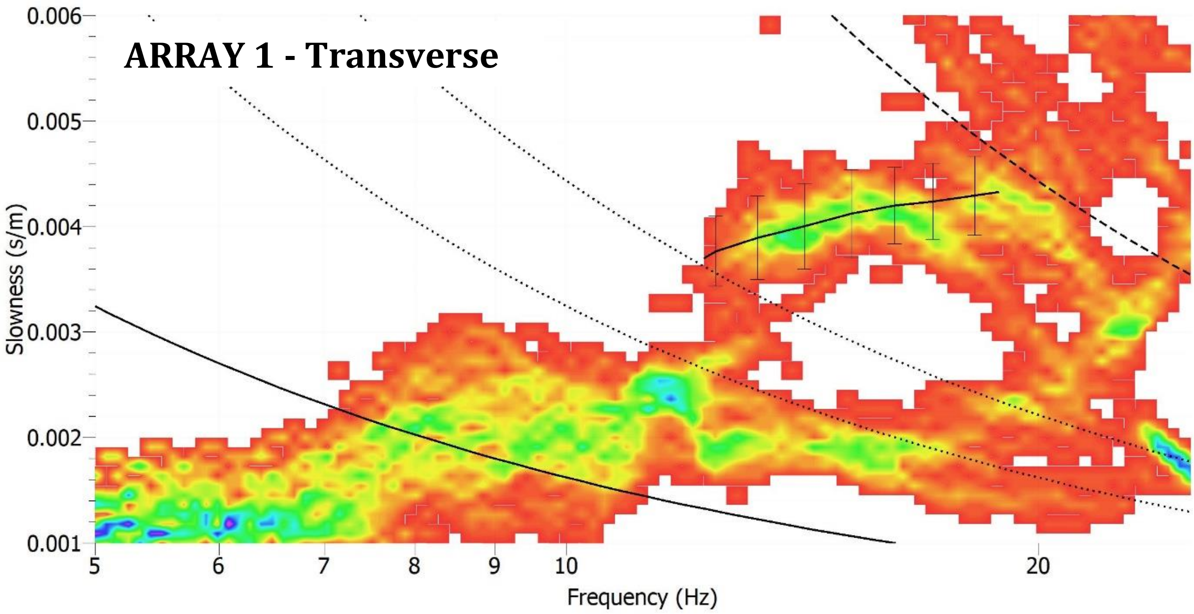

c)

Figure 6: Picked dispersion curve in the slowness domain with the high-resolution FK analysis on the vertical components (a), the radial components (b) and the transverse components (c) of Array 1. The limits for the aliasing conditions are reported with black lines.

The modified spatial autocorrelation technique (MSPAC) has also been applied to the passive data to obtain the autocorrelation curves. Figure 7a shows the 6 rings adopted for the MSPAC analysis on Array 1 and Figure 7b shows the spatial autocorrelation curves computed for each ring.

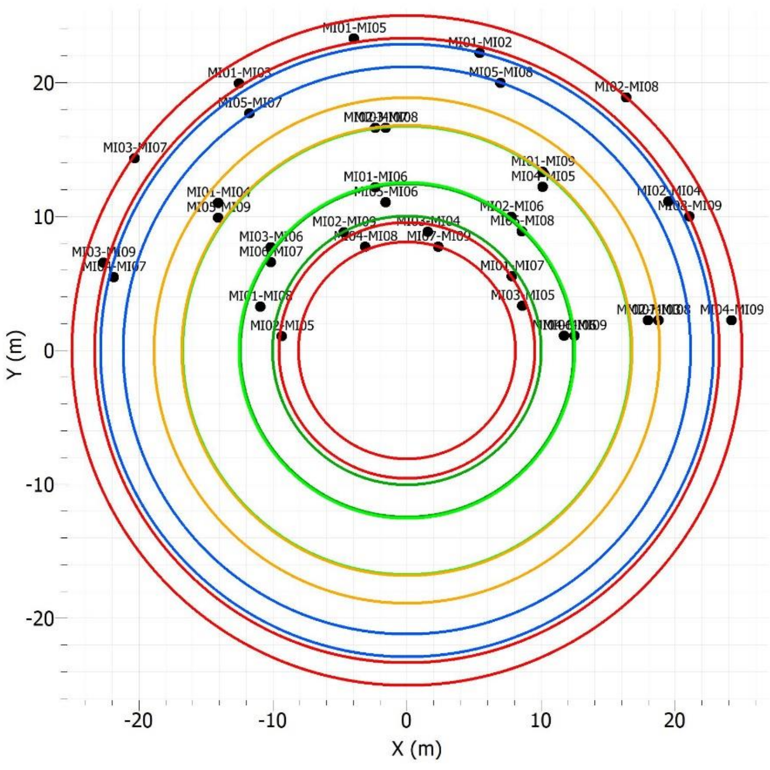

a)

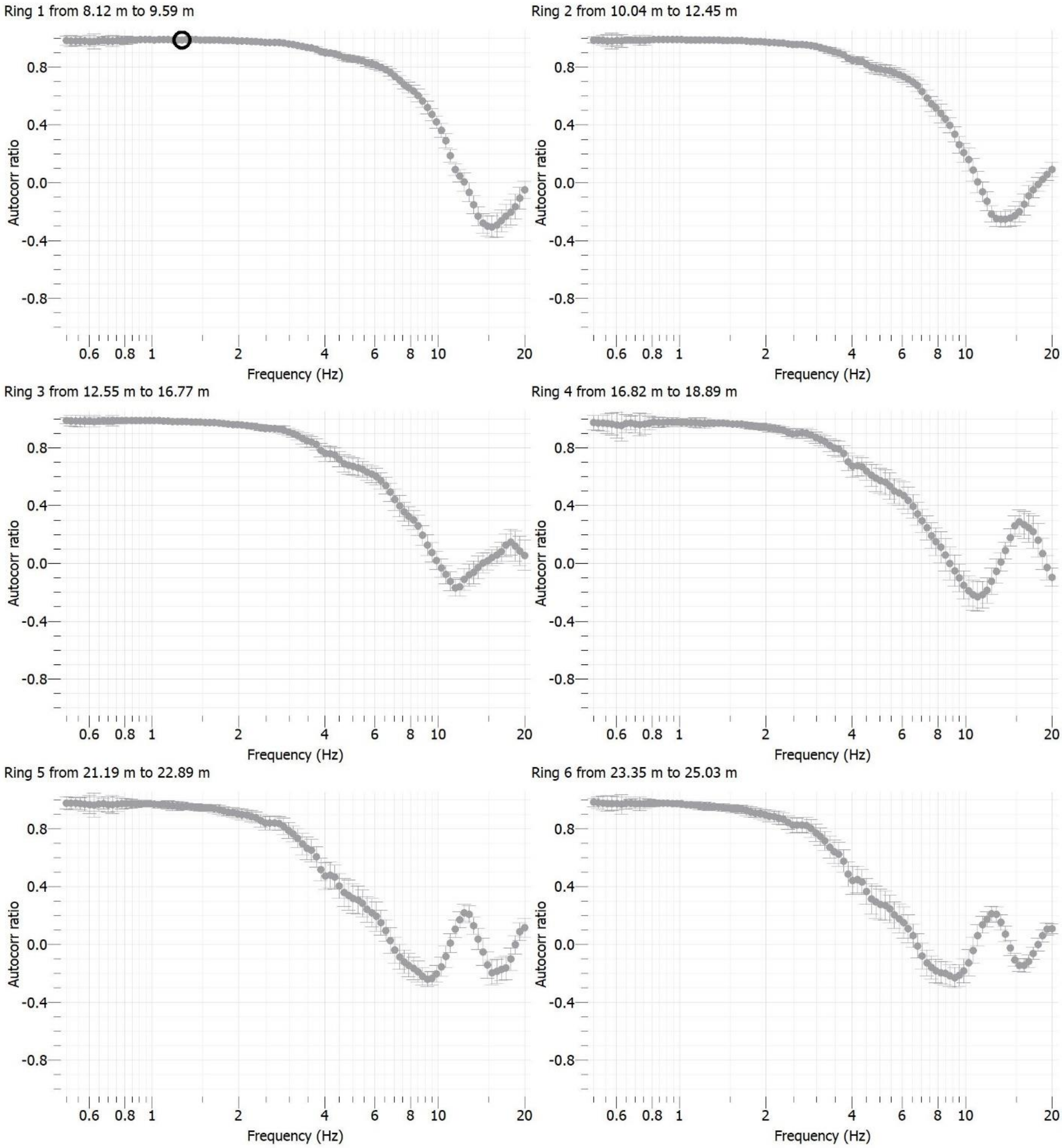

b)

Figure 7: a) rings selected for the MSPAC analysis on Array 1; b) autocorrelation curves of the 6 rings.

The auto-correlation curves in Figure 7b have been inverted to obtain the corresponding Rayleigh wave dispersion curve (Figure 8) in the frequency range 1.7-5 Hz. The black lines indicate the validity range of the picked dispersion curve.

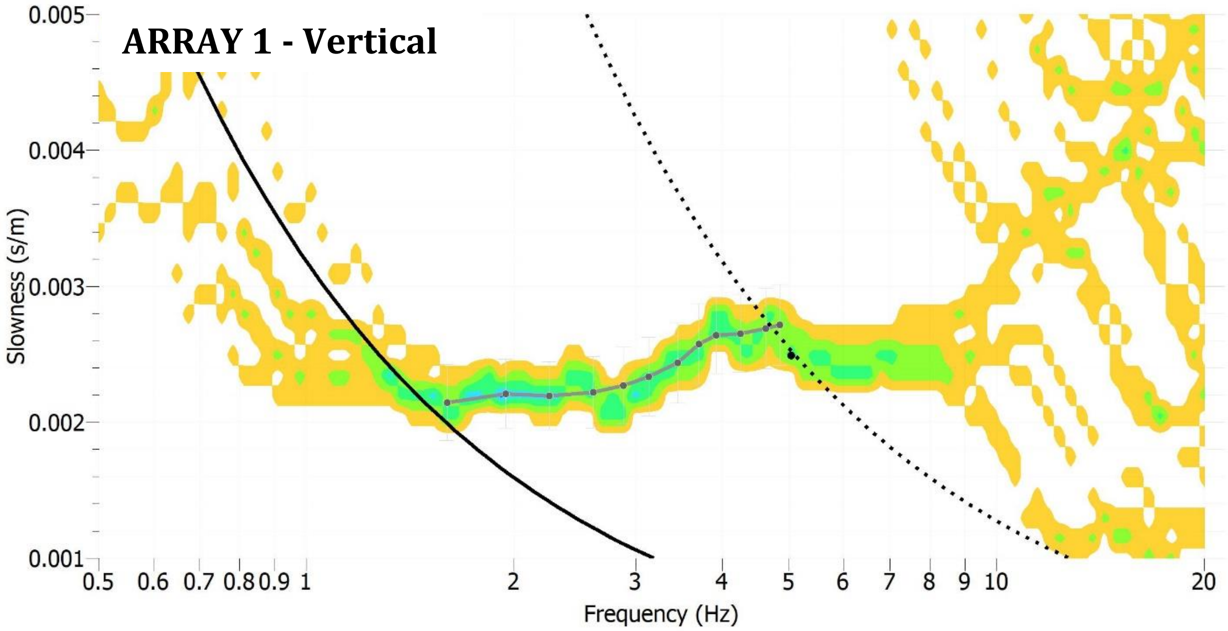

Figure 8: picked dispersion curve in the slowness domain with the MSPAC method on Array 1. The black lines indicate the validity range of the picked dispersion curve.

2.2 ARRAY 2

The geometry of the Array 2 controls the response in terms of theoretical transfer function as described in Figure 9. On the left, the array transfer function is shown. On the right, the limits for the aliasing conditions are reported both in slowness and in velocity domains.

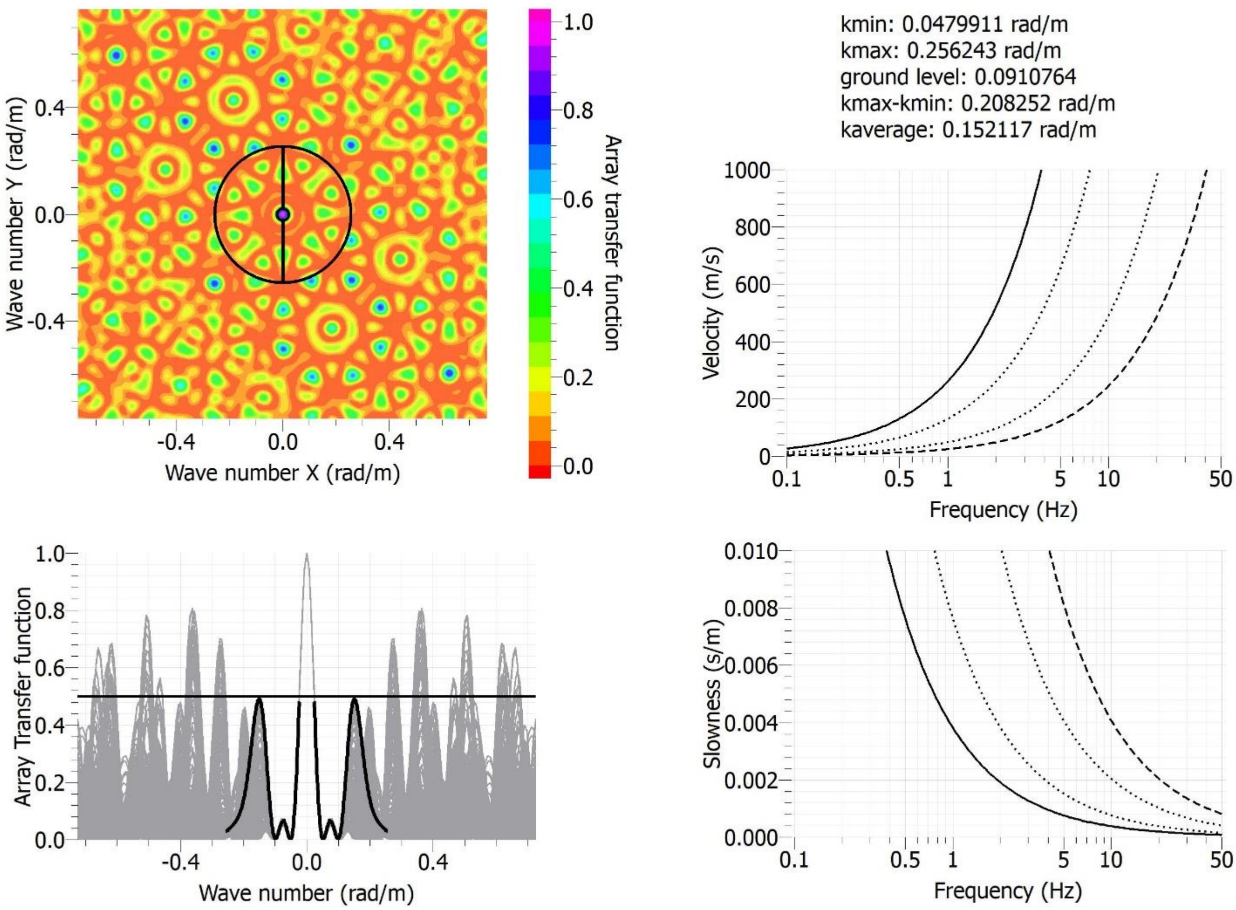

Figure 9: on the left, the theoretical array transfer function is reported for Array 2. On the right, the aliasing conditions are reported in the slowness and velocity domains.

The H/V curves of the 9 stations of Array 2 are superimposed on each other in Figure 10, where the average H/V is reported in a solid black line and the corresponding standard deviation in black dashed lines. As for the Array1, there is a general agreement of the H/V shapes showing a good overlapping in the frequency range 0.1-15 Hz. The H/V peak at 0.18 Hz (σ = 0.03 Hz), already observed from the H/V analyzes on Array 1, is still observed on all the H/V curves from Array2. The directional H/Vs from the 9 stations of Array 2 (Figure 11) do not show any polarization effect.

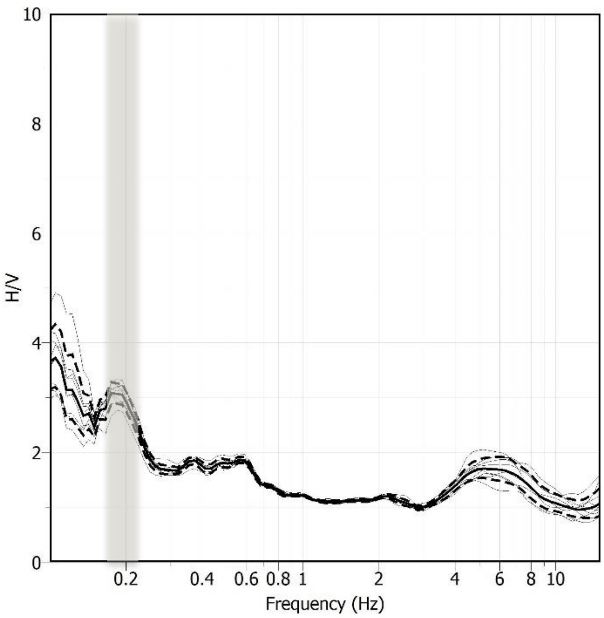

Figure 10: H/V curves of the 9 stations of Array 2. The average is reported in a solid black line, whereas the corresponding standard deviation is reported in dashed black lines.

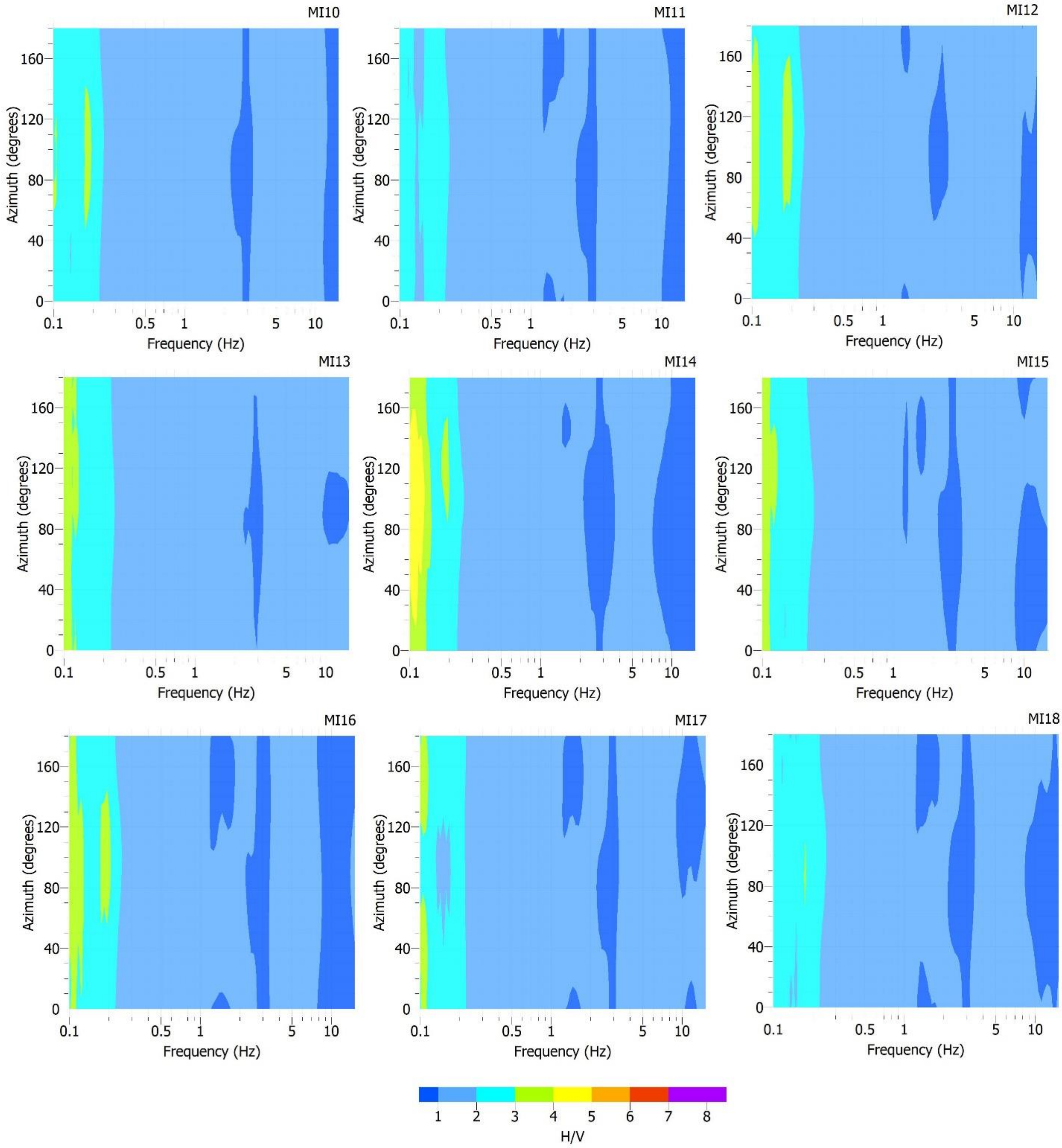

Figure 11: directional H/V for the 9 stations of Array 2.

Data from the 2D array have been analyzed with the GEOPSY code (http://www.geopsy.org) in terms of high-resolution FK analysis on all the three components (NS, EW, Z). The dispersion curves obtained from the Array 2 are shown in Figure 12a for the vertical components, 12b for the radial components and 12c for the transverse components. The vertical and radial components allow picking the Rayleigh wave dispersion curves, whereas the transverse components allow picking the Love wave dispersion curves. The aliasing conditions (black lines) constrain the validity range of the picked dispersion curves in the frequency range 2-12 Hz.

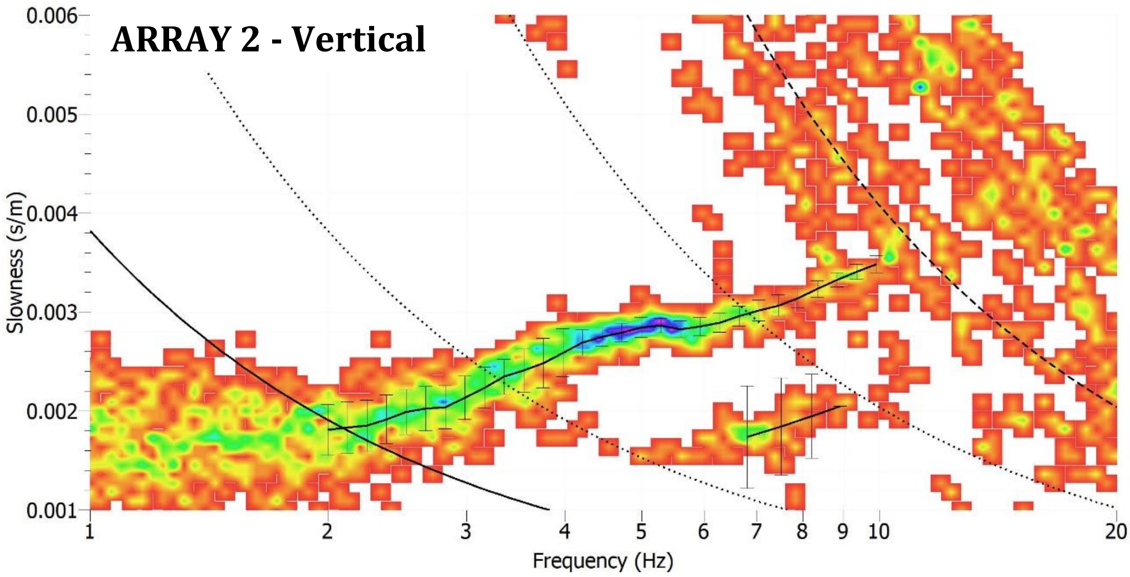

a)

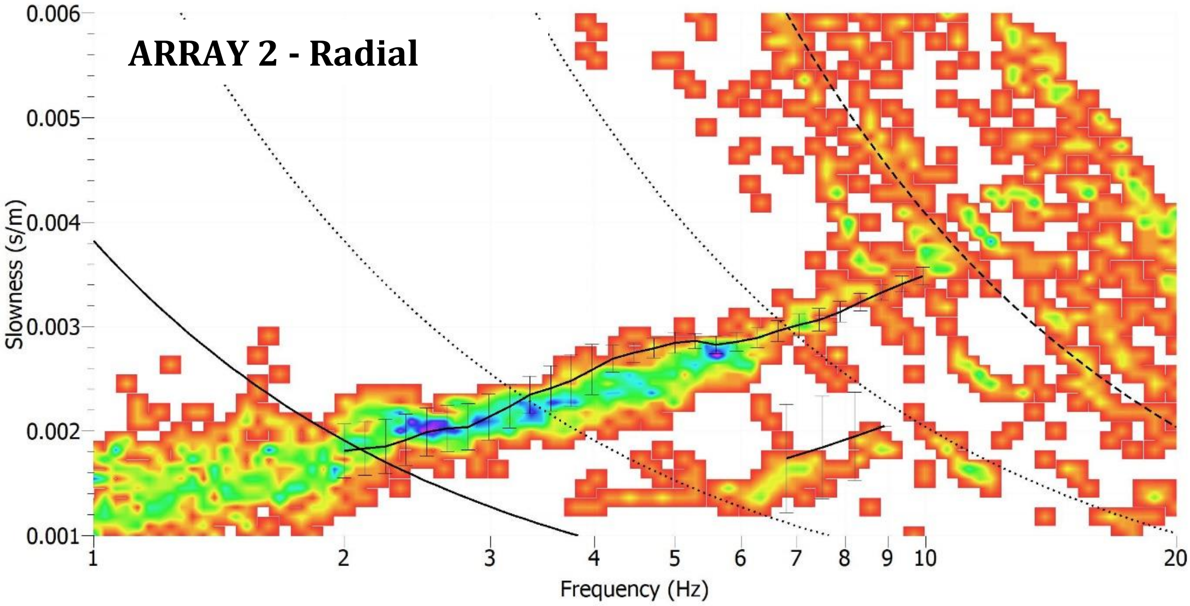

b)

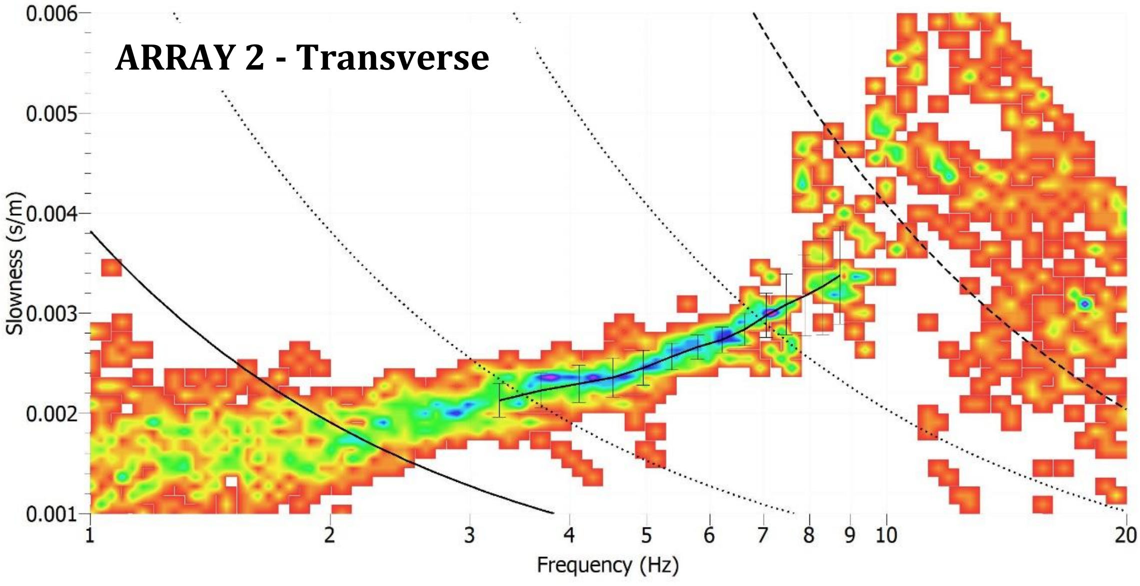

c)

Figure 12: Picked dispersion curve in the slowness domain with the high-resolution FK analysis on the vertical components (a), radial components (b) and transverse components (c) of Array 2. The limits for the aliasing conditions are reported with black lines.

The modified spatial autocorrelation technique (MSPAC) has also been applied to the passive data to obtain the autocorrelation curves. Figure 13a shows the 5 rings adopted for the MSPAC analysis on Array 2 and Figure 13b shows the spatial autocorrelation curves computed for each ring.

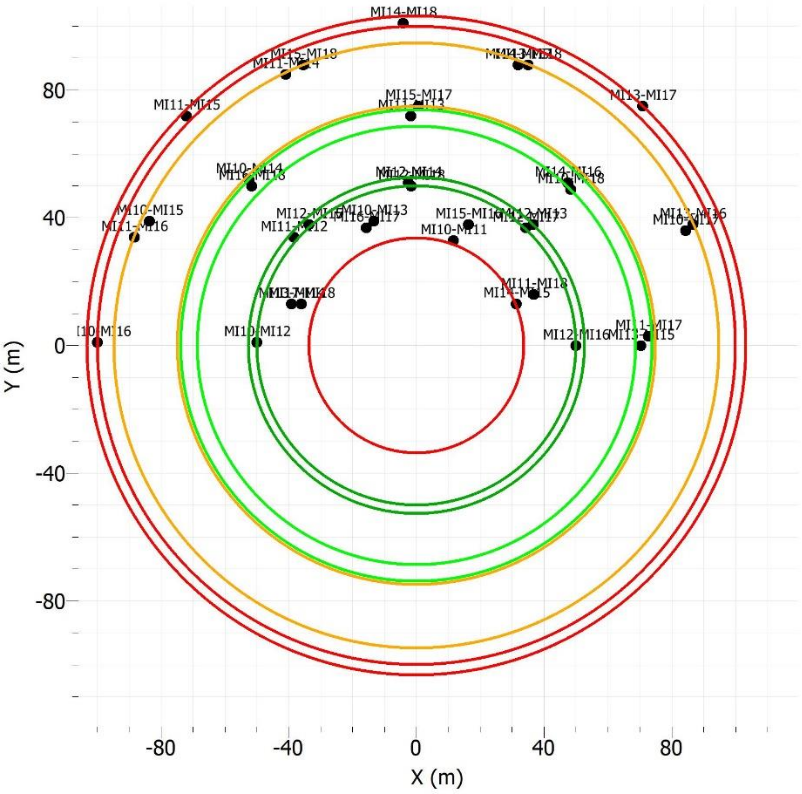

a)

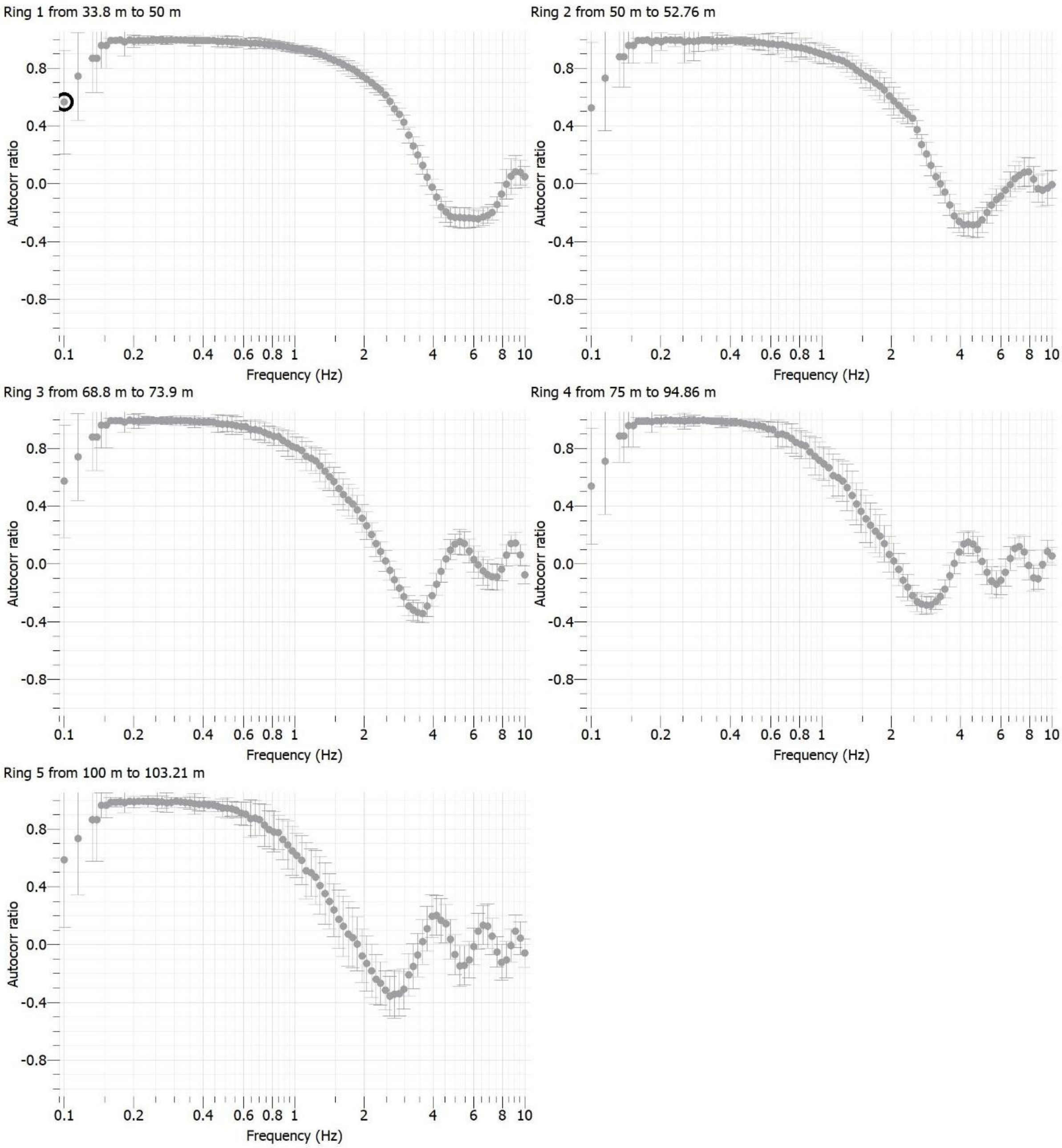

b)

Figure 13: a) rings selected for the MSPAC analysis on Array 2; b) autocorrelation curves of the 5 rings.

The auto-correlation curves in Figure 13b have been inverted to obtain the corresponding dispersion curve in the frequency range 0.38-4 Hz (Figure 14). The black lines indicate the validity range of the picked dispersion curve.

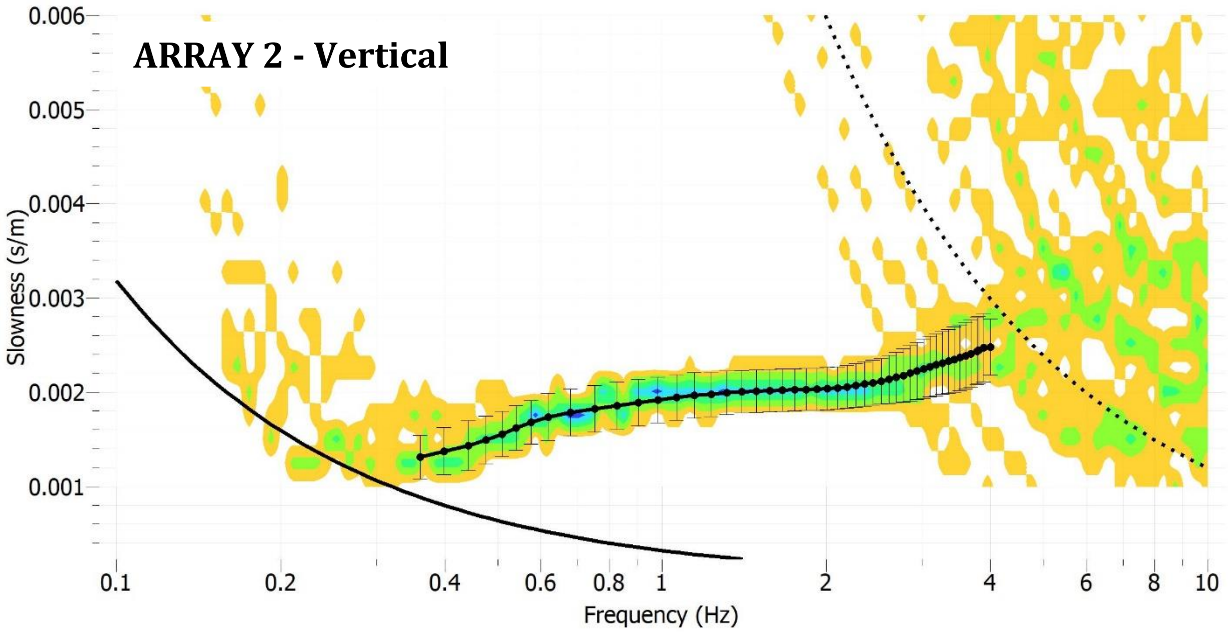

Figure 14: picked dispersion curve in the slowness domain with the MSPAC method on Array 2. The black lines indicate the validity range of the picked dispersion curve.

3. SEISMIC VELOCITY MODEL

Figure 15 compares the dispersion curves obtained from both the FK and MSPAC analyzes on Array 1 and Array 2. Figure 15a shows all the Rayleigh wave dispersion curves, whereas Figure 15b shows all the Love wave dispersion curves. Even if we observe a good consistency between the different curves, they have to be interpreted in order to assign the relative mode (fundamental mode or higher modes). This interpretation is made by performing several inverse models with different initial assumptions on all the dispersion curves. The inverse model that could fit with the lowest misfit the highest number of curves is the one selected to define the Vs profile, with the corresponding initial assumptions on the different dispersion curves.

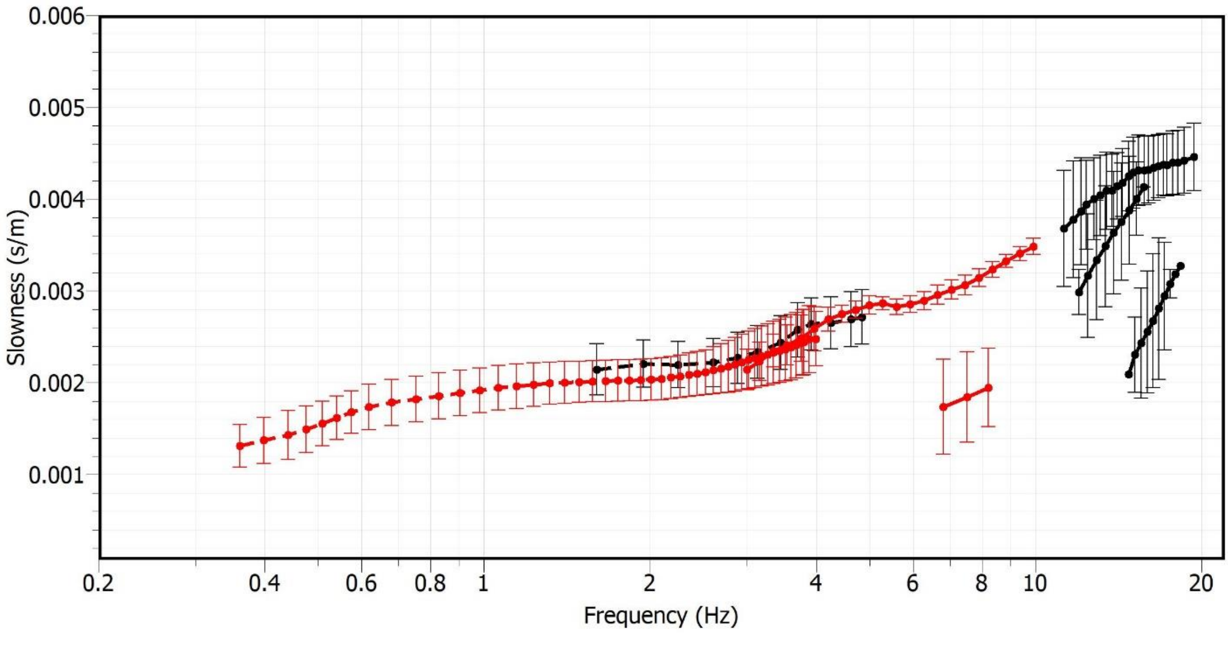

a)

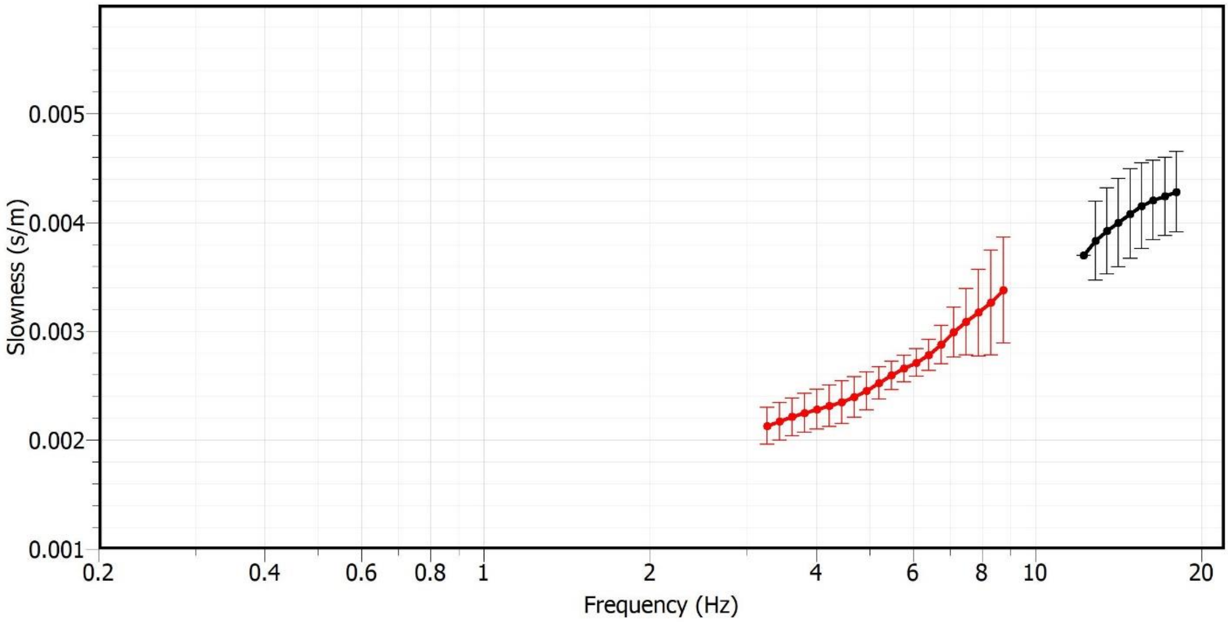

b)

Figure 15: Rayleigh wave dispersion curves (a) and Love wave dispersion curves (b) from both Array 1 (in black) and Array 2 (in red). The curves obtained from f-k methods are reported in solid lines, whereas those obtained from the MPSAC method are reported in dashed lines.

To proceed with the inversion, we estimate the ellipticity curve from the H/V curve, considering in particular the right flank of the H/V peak that carries the important information on the underground structure. To reduce the contribution of the other waves in the H/V flanks, a common practice consists in reducing the H/V amplitude for the square root of 2 (Foti et al., 2011). The estimated ellipticity curve is reported in Figure 16 (blue curves) together with the average H/V curve (black curve).

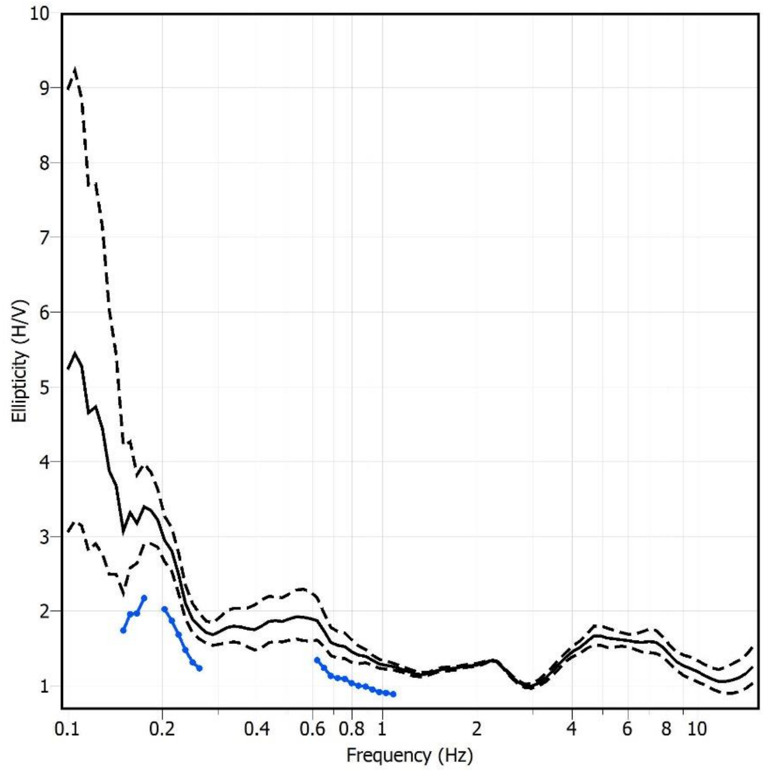

Figure 16: estimation of the ellipticity curve (blue) from the average H/V curve (black) of Array 1.

Finally, we jointly invert the following targets:

1) Rayleigh wave dispersion curves (fundamental and higher modes) in Figure 15a
2) Love wave dispersion curves in Figure 15b
3) ellipticity curve in Figure 16 (blue curves)

The fit between the experimental and theoretical curves is shown in Figure 17. The Rayleigh wave dispersion curves are interpreted and assumed to be relative to the fundamental mode, besides the first, second and third higher modes (Figure 17a). On the other hand, the Love wave dispersion curves are interpreted and assumed to be relative to the first higher mode.

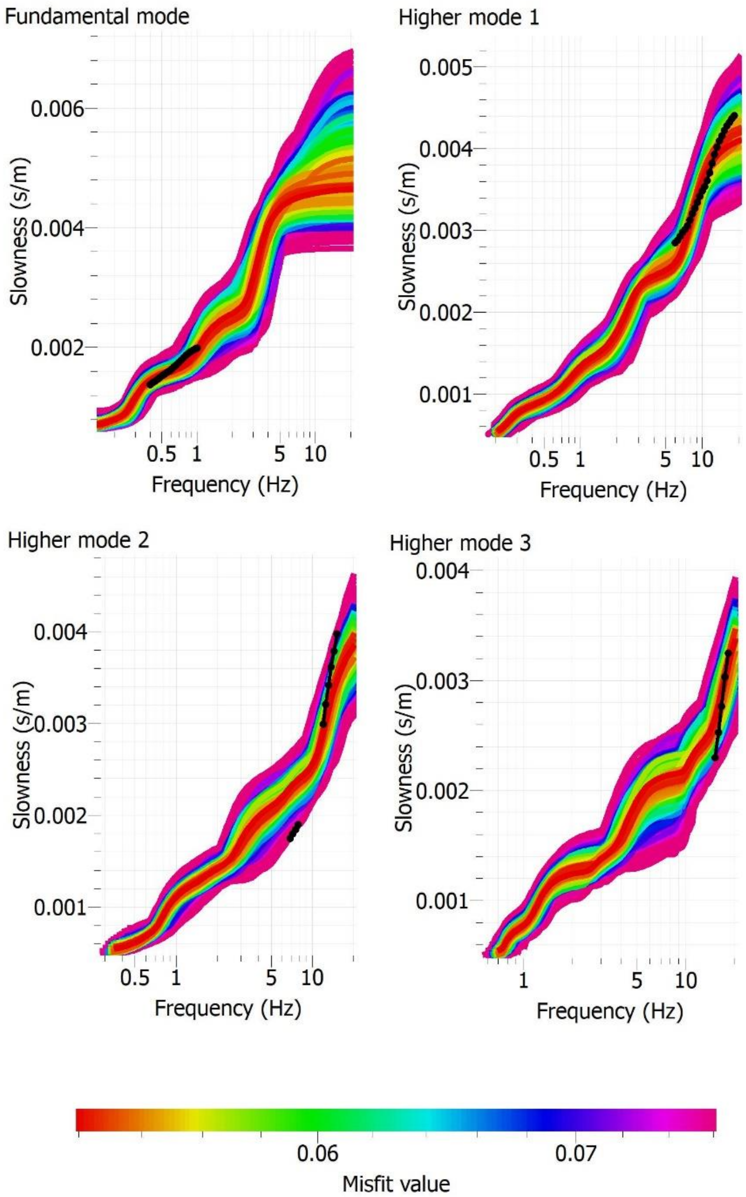
Fundamental mode
Slowness (s/m)
0.006
0.004
0.002
0.5 1 5 10
Frequency (Hz)
Higher mode 1
0.005
0.004
0.003
0.002
0.001
Higher mode 2
Higher mode 3
0.06
0.07
Misfit value

a)

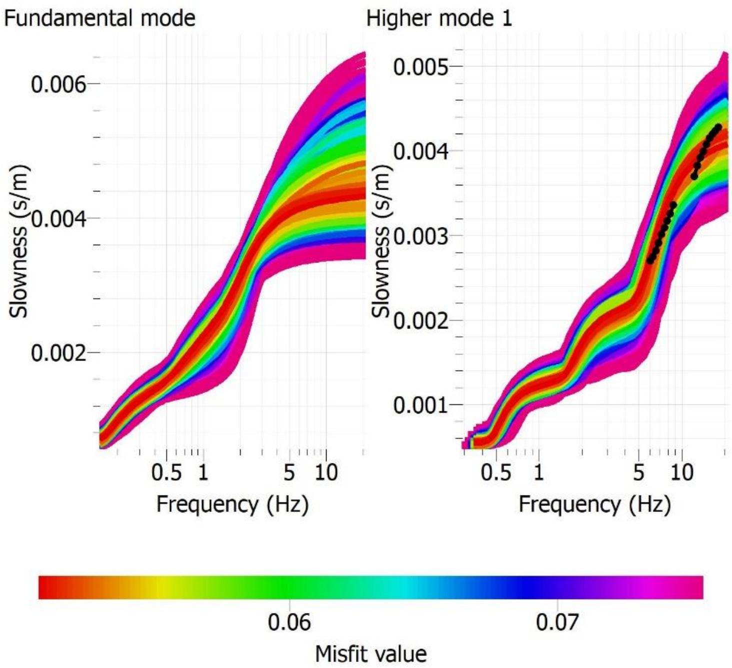
Fundamental mode
Higher mode 1
Slowness (s/m)
0.006
0.004
0.002
0.005
0.003
0.001
Frequency (Hz)
0.5 1 5 10
0.06
0.07
Misfit value

b)

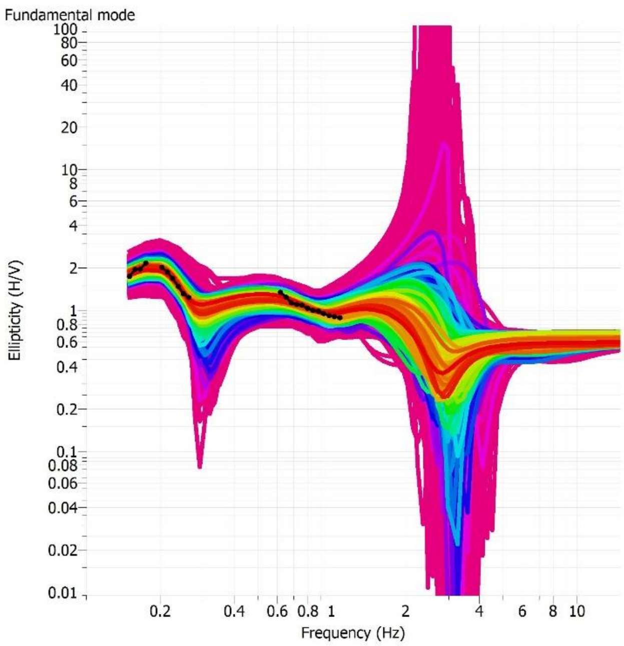
Fundamental mode
Ellipticity (H/V)
100
80
60
40
20
10
8
6
4
2
1
0.8
0.6
0.4
0.2
0.1
0.08
0.06
0.04
0.02
0.01
0.2 0.4 0.6 0.8 1 2 4 6 8 10
Frequency (Hz)
0.06
0.07
Misfit value

c)

Figure 17: Joint inversion of the Rayleigh wave dispersion curves (a) and Love wave dispersion curves (b) obtained from the array measurements (Array 1 and Array 2) with the additional constrain of the estimated ellipticity curve (c). The field data are reported with black curves.

A fairly good fit is obtained between experimental and theoretical curves using a model parameterization composed of four layers over halfspace. The *Vs* profile obtained from the inversion process is reported in Figure 18a, with a zoom on the shallow structure in Figure 18b. The results indicate shallow soft layers with thickness <40 m and *Vs* around 230 m/s. A deeper layer shows *Vs* of 457 m/s down to 190 m in depth, where a another layer is characterized by *Vs* values around 800 m/s. The halfspace is found at 1110 m in depth with Vs of 1824 m/s.

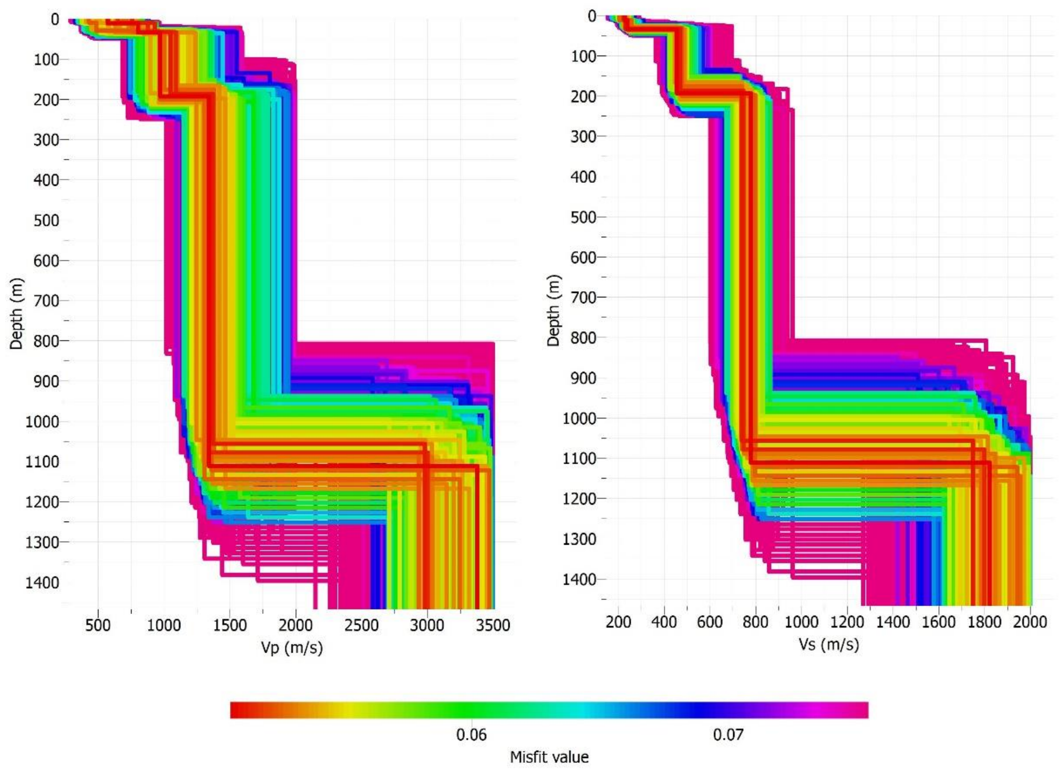

a)

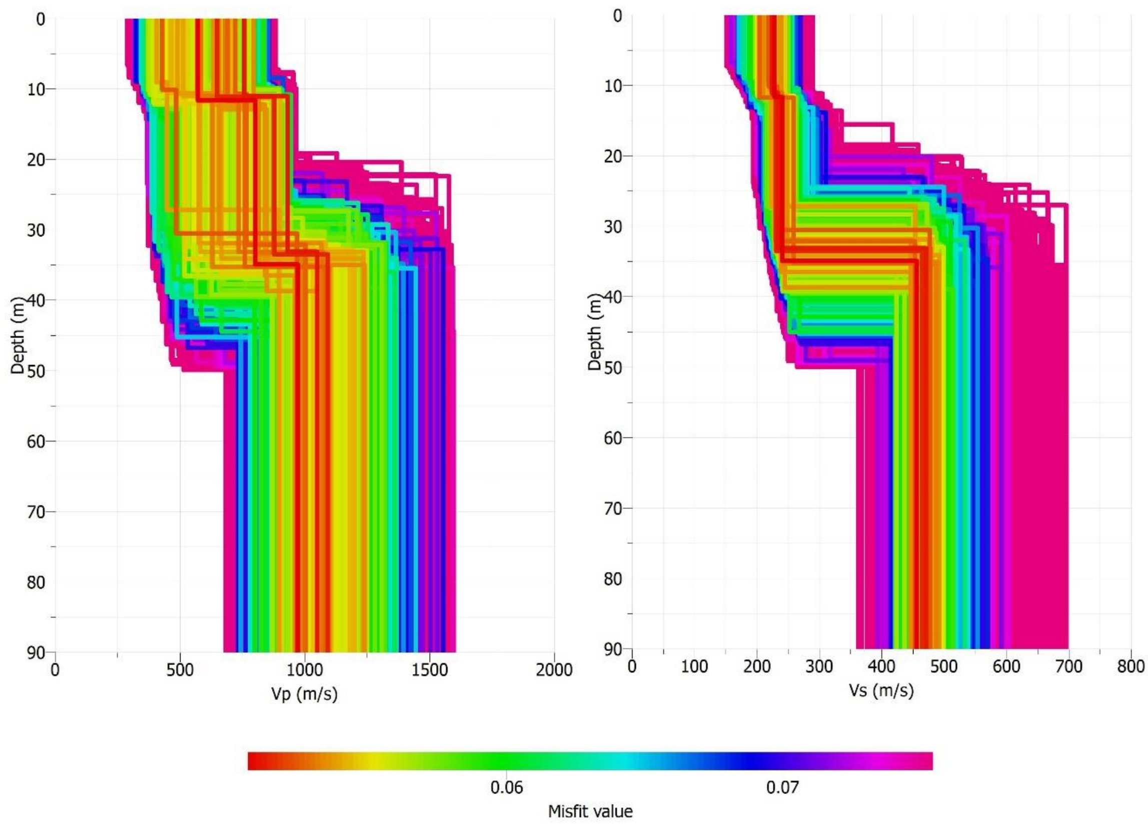

b)

Figure 18: a) Vs profile obtained from the joint inversion of dispersion and ellipticity curves in Figure 17. b) Zoom on the shallow structure of the Vs profile.

The best Vp and Vs models (i.e. lowest misfit) resulting from the inversion process are proposed in Figure 19. The corresponding values are reported in Table 3.

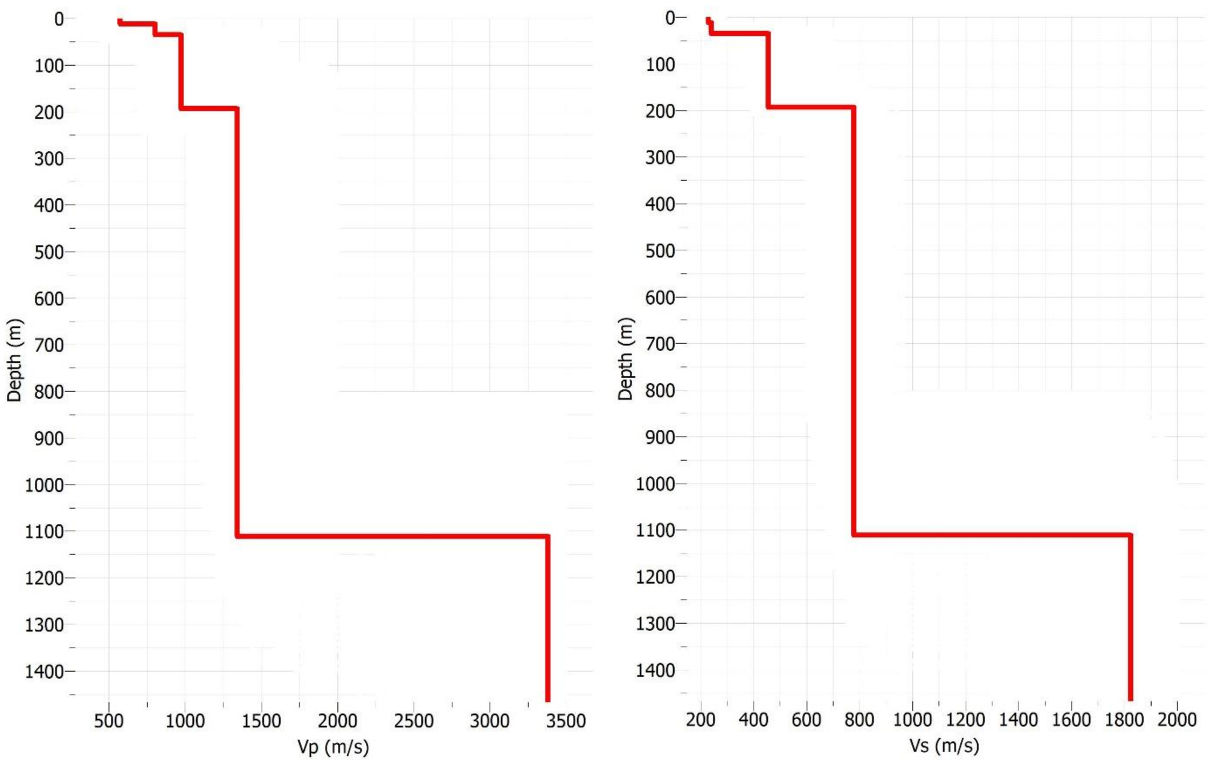

Figure 19: Best-fit models of Vp (left panel) and Vs (right panel) values.

From	*To*	*Thickness [m]*	*V_S [m/s]*	*V_P [m/s]*
0	10	10	226	569
10	36	26	241	801
36	190	154	457	970
190	1110	920	779	1341
1110	?		1824	3376

Table 3: Best-fit models

4. CONCLUSIONS

Geophysical measurements executed at the IV.MILN seismic station consist in two ambient-vibration arrays in 2D configuration.

The H/V analyzes executed on the array measurements indicate one main resonant peak at 0.18 Hz, in agreement with the H/V analysis at the IV.MILN seismic station (INGV-CRISP project, 2015-2016). A further mild amplification in the frequency range 0.4-0.6 Hz is observed on the H/V curves from Array 1. The directional HV from both Array1 and Array2 do not show any significant polarization effect in the analyzed frequency range 0.1-15 Hz.

To assess the Vs profile at the site, a joint inversion of the Rayleigh wave and Love wave dispersion curves was performed, with the additional constrain of the estimated ellipticity curve. The Vs profile was subsequently correlated to the stratigraphic model provided in the geological report at IV.MILN (Working group INGV (2019). Geological report at the seismic station IV.MILN), showing a good correlation in the first 90 m of the subsoil (Figure 20). A first layer with thickness <40 m and *Vs* around 230 m/s correlates with the gravel and sand layer belonging to the Guanzate Unit (Working group INGV (2019). Geological report at the seismic station IV.MILN), whereas a further layer with *Vs* of 457 m/s correlates with a subsequent predominant sand layer (Figure 20).

The Vs profile obtained in this study also indicates a further velocity discontinuity at around 190 m in depth, in correspondence to the base of the Quaternary continental sediments (i.e., R-Surface, Working group INGV (2019). Geological report at the seismic station IV.MILN), where the shear-wave velocity moves from 457 m/s to 779 m/s (referring to the best-fit model of Figure 19). This discontinuity is constrained with the mild H/V peak at 0.6 Hz. Moreover, a deeper velocity discontinuity is observed at 1110 m in depth, in correspondence to the base of the Quaternary marine sedimentation (Working group INGV (2019). Geological report at the seismic station IV.MILN), where the shear-wave velocity reach around 1800 m/s. This deeper discontinuity is constrained with the H/V peak at 0.18 Hz.

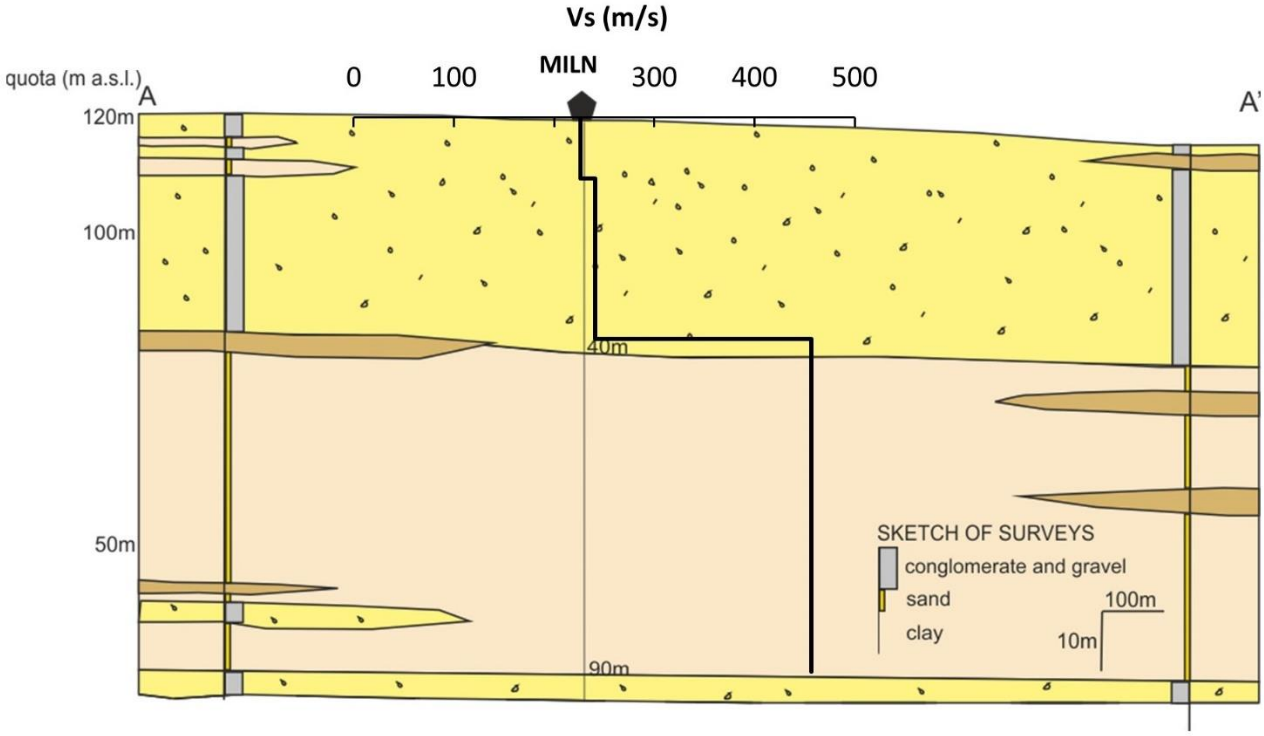

Figure 20: correlation between geological and geophysical information at the IV.MILN site (geological section from Working group INGV (2019). Geological report at the seismic station IV.MILN – Milano).

According to the current Italian seismic code (NTC 2018), if the bedrock (Vs > 800 m/s) is more than 30 m in depth, the equivalent velocity ($V_{s,eq}$) is equal to the $V_{S,30}$. This is the case of the IV.MILN site, where the $V_{S,30}$ computed from the available *Vs* profile is 236 m/s, and the site is classified in the soil category C for both the NTC18 and EC8 seismic classifications (Table 4).

$V_{s,eq} = V_{S,30}$ (m/s)	*Soil class (NTC 2018)*	*Soil class (EC8)*
236	C	C

Table 4: Soil Class

REFERENCES

EC8: European Committee for Standardization (2004). Eurocode 8: design of structures for earthquake resistance. P1: General rules, seismic actions and rules for buildings. Draft 6, Doc CEN/TC250/SC8/N335.

Foti, S., S. Parolai, D. Albarello, and M. Picozzi (2011). Application of surface-wave methods for seismic site characterization, Surv. Geophys. 32, no. 6, 777–825.

INGV-CRISP project, "CaRatterIzzazione dei sIti delle stazioni Sismiche Permanenti INGV" (Coordinators: Paola Bordoni e Giovanna Cultrera). Linea di attività INGV-T3 "Pericolosità sismica e contributi alla definizione del rischio", 2015-16; Convenzione DPC-INGV 2016-17-18, Allegato B2: Obiettivo 1 - TASK B: "Caratterizzazione siti accelerometrici".

NTC 2018: Ministero delle Infrastrutture e dei Trasporti (2018). Aggiornamento delle Norme Tecniche per le Costruzioni. Part 3.2.2: Categorie di sottosuolo e condizioni topografiche, Gazzetta Ufficiale n. 42 del 20 febbraio 2018 (in Italian).

SESAME Project (2004). SESAME Guidelines, European Research Project WP12 – Deliverable D23.12.

Working group INGV "Agreement DPC-INGV 2019-21. All.B2 – WP1, Task 2", (2019). Geological report at the seismic station IV. MILN – Milano. http://hdl.handle.net/2122/12935

1This document is level 3 as defined in the "Principi della politica dei dati dell'INGV (D.P. n. 200 del 26.04.2016)"

Esclusione di responsabilità e limiti di uso delle informazioni

L'INGV, in ottemperanza a quanto disposto dall'Art.2 del D.L. 381/1999, svolge funzioni di sorveglianza sismica e vulcanica del territorio nazionale, provvedendo all'organizzazione della rete sismica nazionale integrata e al coordinamento delle reti sismiche regionali e locali in regime di convenzione con il Dipartimento della Protezione Civile.

L'INGV concorre, nei limiti delle proprie competenze inerenti la valutazione della Pericolosità sismica e vulcanica nel territorio nazionale e secondo le modalitaà concordate dall'Accordo di programma decennale stipulato tra lo stesso INGV e il DPC in data 2 febbraio 2012 (Prot. INGV 2052 del 27/2/2012), alle attività previste nell'ambito del Sistema Nazionale di Protezione Civile.

In particolare, questo documento1 ha finalità informative circa le osservazioni e i dati acquisiti dalle Reti di monitoraggio e osservative gestite dall'INGV.

L'INGV fornisce informazioni scientifiche utilizzando le migliori conoscenze scientifiche disponibili al momento della stesura dei documenti prodotti; tuttavia, in conseguenza della complessità dei fenomeni naturali in oggetto, nulla può essere imputato all'INGV circa l'eventuale incompletezza ed incertezza dei dati riportati.

L'INGV non è responsabile dell'utilizzo, anche parziale, dei contenuti di questo documento da parte di terzi e di eventuali danni arrecati a terzi derivanti dal suo utilizzo.

La proprietà dei dati contenuti in questo documento è dell'INGV.

1Questo documento rientra nella categoria di livello 3 come definita nei "Principi della politica dei dati dell'INGV (D.P. n. 200 del 26.04.2016)".